Int. J. Solids Structures Vol. 29, No. 24, pp. 3201-3220, 1992
Printed in Great Britain.

0020-7683/92 $5.00 + .00

BOUNDARY ELEMENT ANALYSIS OF INTERFACE CRACKS BETWEEN DISSIMILAR ANISOTROPIC MATERIALS

C. L. TAN, Y. L. GAO and F. F. AFAGH
Department of Mechanical and Aerospace Engineering, Carleton University, Ottawa, Canada K1S 5B6

(*Received* 16 *September* 1991; *in revised form* 30 *April* 1992)

Abstract—In this paper, the boundary element method (BEM) is applied to the analysis of interface cracks between dissimilar anisotropic materials in plane elasticity. It is based on the quadratic element formulation and special crack-tip elements which incorporate the proper $O(r^{-1/2+i\gamma})$ oscillatory traction singularity are employed. A simple expression relating the stress intensity factors to the BEM computed traction coefficients is derived, and this procedure for determining stress intensity factors is validated by several examples. The numerical results obtained are shown to be very satisfactory even with relatively coarse mesh discretizations.

1. INTRODUCTION

The study of cracks that lie along the interface between two different elastic media is important in providing a better understanding of the integrity of bonded interfaces between dissimilar materials, and for determining the appropriate factors which affect the mechanical properties of composites and multi-phase solids. In such problems, the near-tip fields may be characterized by the complex stress intensity factor $\mathbf{K} = K_{\mathrm{I}} + iK_{\mathrm{II}}$, and the stresses in the vicinity of the interface crack tip are oscillatorily singular, of the order $r^{-1/2+i\gamma}$, where γ is a bimaterial property. Also, the tensile and shear effects are always coupled, even for single mode loading. As a result, the stress intensity factors (S.I.F.), K_{I} and K_{II}, should not be interpreted in the classical separate sense as for cracks in homogeneous materials.

The bimaterial interface crack problem has been the subject of extensive theoretical and experimental investigations in recent years [e.g. Rice (1988), Hasebe *et al.* (1987), Kacznski and Matysiak (1989), Comninou (1990), Charalambides *et al.* (1989), Sun and Jih (1987), Matos *et al.* (1989), Hutchinson and Evans (1989), Yehia and Sheppard (1988), Toya (1990), Park and Earmme (1986) and Cao and Evans (1989)], although it has previously also received some attention by Williams (1959), Erdogan (1965), England (1965), Rice and Sih (1965), Perlman and Sih (1967) and Comninou (1977), among others. However, these studies based on the linear elastic fracture mechanics approach have concentrated mainly on isotropic bimaterials; similar investigations into anisotropic bimaterials are relatively limited in number. Reported works in this latter case include those by Willis (1971), Clements (1971), Ting (1986), Bassani and Qu (1989a, b), Wu (1990, 1991), Ni and Nemat-Nasser (1991) and Nakagawa *et al.* (1990), all of whom have treated the problem analytically. Numerical methods have also been employed for the analysis of interface cracks between non-isotropic elastic media, but the finite element method is the technique almost exclusively used. Among the contributions in this regard are those by Wang and Yuan (1983), Kuo and Wang (1985), Raju *et al.* (1988), Sun and Manoharan (1989), and Lin and Hartmann (1989).

The boundary element method (BEM), also commonly known as the boundary integral equation (BIE) method, has recently been applied to the study of interface cracks as well, but only in isotropic bimaterials [Yuuki *et al.*, 1987; Yuuki and Cho, 1989; Lee and Choi, 1988; Tan and Gao, 1990a, b, 1991; Gao and Tan, 1992). In the BEM approach employed by Yuuki *et al.* (1987) and Yuuki and Cho (1988), Hetenyi's solution for a point load in an infinite plate made of two dissimilar isotropic media was used as the fundamental solution in the BIE formulation. The stress intensity factors, K_{I} and K_{II}, were then obtained by extrapolation techniques based on the computed crack face displacement data. Lee and

Choi (1988), on the other hand, used the conventional formulation of the BEM with quadratic isoparametric elements. They obtained the stress intensity factors by directly correlating the computed nodal displacements on the elements adjacent to the interface crack-tip to the classical field solution. In both these approaches, however, very refined mesh discretizations, by conventional BEM standards, need to be employed. Tan and Gao (1990a, b, 1991) and Gao and Tan (1992) also used the conventional BEM in their studies, but with quarter-point $O(r^{-1/2})$ traction-singular crack-tip elements. Instead of computing for K_I and K_{II} directly, the modulus, K_0, of the complex stress intensity factor, which may also be written as $\mathbf{K} = K_0 e^{i\psi}$, was obtained. It is worth mentioning here that for the interface crack in isotropic bimaterials, this quantity K_0 is directly related to the strain energy release rate. In these references, the authors calculated K_0 from expressions they had derived relating it to the computed nodal tractions or to the nodal displacements of the quarter-point crack-tip elements. The phase, ψ, of the complex stress intensity factor, however, was not determined directly using a formally established procedure. Instead, it was estimated via its relationship with the crack face displacements at certain positions on the crack-tip elements. These positions were established from numerical experiments carried out on several test problems with exact analytical solutions. Nevertheless, good solution accuracy for K_0 and ψ was obtained even with relatively coarse mesh designs.

In this paper, the conventional BEM with quarter-point crack-tip elements is applied to the analysis of interface cracks between two dissimilar anisotropic media in two dimensions. In contrast to the previous treatment by the authors on interface cracks in isotropic bimaterials mentioned above, the proper $O(r^{-1/2+i\varepsilon})$ traction singularity is incorporated in the crack-tip elements employed. Also, instead of obtaining K_0 and ψ, the focus of the study is the direct determination of K_I and K_{II}. This is because, as will be evident later, any expression for K_0 in terms of the computed primary variables, namely, the displacements and the tractions, becomes significantly more complicated in the anisotropic case, and it is also doubtful if the less than formal procedure to estimate the phase angle ψ of the complex stress intensity factor remains applicable. Moreover, the relationship between the strain energy release rate and K_0 is no longer as direct and simple as before. In this study, analytical expressions which enable K_I and K_{II} to be calculated directly from the computed nodal tractions on the crack-tip elements are derived. The veracity of the present approach is demonstrated by several examples involving an interface crack in isotropic and anisotropic bimaterials. Before these results are presented and discussed, the analytical basis of the method employed will first be shown.

2. BASIC EQUATIONS AND THE S.I.F.

The development of the equations presented here closely follows that by Bassani and Qu (1989) and Wu (1990). The indicial notation is used, in which the Latin indices take on the values 1, 2 and 3 while the Greek indices only take on the values 1 and 2. Also, summation is implied for repeated indices.

For a generally anisotropic elastic body in Cartesian co-ordinate space x_j, the stress–strain relation may be written as

$$\sigma_{kl} = C_{klmn}\varepsilon_{mn} \tag{1}$$

and the Navier's equation of equilibrium for plane deformation of the body as

$$C_{k\alpha m\beta}u_{m,\alpha\beta} = 0, \tag{2}$$

where u_m, σ_{kl} and ε_{mn} are the displacements, stresses and strains, respectively, and C_{klmn} are the elastic constants of the material. By introducing the following Fourier transform pair:

$$\tilde{f}(\xi) = \frac{1}{\sqrt{2\pi}} \int_{-\infty}^{\infty} f(x)\, e^{i\xi x}\, dx, \tag{3a}$$

$$f(x) = \frac{1}{\sqrt{2\pi}} \int_{-\infty}^{\infty} \tilde{f}(\xi)\, e^{-i\xi x}\, d\xi, \tag{3b}$$

where $i = \sqrt{-1}$, and applying them to eqn (2) over the x_1 co-ordinate, the following equation may be obtained:

$$\xi_1^2 C_{j1k1}\tilde{u}_k + j\xi_1 (C_{j2k1} + C_{j1k2}) \frac{\partial \tilde{u}_k}{\partial x_2} - C_{j2k2} \frac{\partial^2 \tilde{u}_k}{\partial x_2^2} = 0. \tag{4}$$

This equation may also be written in matrix notation as

$$\xi_1^2 \mathbf{Q}\tilde{\mathbf{u}} + j\xi_1 (\mathbf{S} + \mathbf{S}^T) \frac{\partial \tilde{\mathbf{u}}}{\partial x_2} - \mathbf{V} \frac{\partial^2 \tilde{\mathbf{u}}}{\partial x_2^2} = 0, \tag{5}$$

where the superscript "T" denotes the transpose of the matrix and

$$\mathbf{Q} = (Q_{jk}) = (C_{j1k1}) = \begin{bmatrix} C_{1111} & C_{1112} & C_{1113} \\ C_{1211} & C_{1212} & C_{1213} \\ C_{1311} & C_{1312} & C_{1313} \end{bmatrix}, \tag{6a}$$

$$\mathbf{S} = (S_{jk}) = (C_{j1k2}) = \begin{bmatrix} C_{1111} & C_{1122} & C_{1123} \\ C_{1212} & C_{1222} & C_{1223} \\ C_{1312} & C_{1322} & C_{1323} \end{bmatrix}, \tag{6b}$$

$$\mathbf{V} = (V_{jk}) = (C_{j2k2}) = \begin{bmatrix} C_{1212} & C_{1222} & C_{1223} \\ C_{2212} & C_{2222} & C_{2223} \\ C_{2312} & C_{2322} & C_{2323} \end{bmatrix}. \tag{6c}$$

Equation (4) or (5) admits particular solutions of the form

$$\tilde{u}_k(\xi_1) = a_k(\xi_1)\, e^{-i\xi_2 x_2}, \tag{7}$$

or, in matrix notation,

$$\tilde{\mathbf{u}} = \mathbf{a}(\xi_1)\, e^{-i\xi_2 x_2} \tag{8}$$

provided that $\mathbf{a}$ and ξ_2 satisfy the eigenvalue equation

$$[\xi_1^2 \mathbf{Q} + \xi_1 \xi_2 (\mathbf{S} + \mathbf{S}^T) + \xi_2^2 \mathbf{V}]\mathbf{a}(\xi_1) = 0. \tag{9}$$

If $\xi_2 = p\xi_1$, eqn (9) becomes

$$[\mathbf{Q} + p(\mathbf{S} + \mathbf{S}^T) + p^2 \mathbf{V}]\mathbf{a}(\xi_1) = 0 \tag{10}$$

and the necessary and sufficient condition for $\mathbf{a}$ not having trivial solutions is thus the vanishing of the determinant of the coefficient matrix in eqn (10). That is

$$|\mathbf{Q} + p(\mathbf{S} + \mathbf{S}^T) + p^2 \mathbf{V}| = 0, \tag{11}$$

which is a sixth-order polynomial in p. Since $\mathbf{Q}$, $\mathbf{S}$ and $\mathbf{V}$ are real and are functions of the

material constants C_{ijmn}, the roots p_N $(N = 1, 6)$, are independent of ξ_1. And because eqn (2) is elliptic, eqn (11) has three pairs of complex conjugate roots. Thus the six roots may be written as

$$\mathrm{Im}(p_M) > 0, \quad p_{M+3} = \overline{p_M}, \quad M = 1, 3. \tag{12}$$

Consider now a crack lying along the interface between two semi-infinite solids which are made of linear elastic anisotropic materials I and II, respectively, as shown in Fig. 1. In the vicinity of the crack-tip, the stresses ahead of the crack along the interface are written as

$$\mathbf{t} = t_i = (\sigma_{12} \quad \sigma_{22} \quad \sigma_{32})^{\mathrm{T}}. \tag{13}$$

From dimensional considerations [see Rice (1988)], the stress intensity factors for interface cracks may also be written with reference to a characteristic dimension, say L, of the physical problem. These stress intensity factors will be written as

$$\mathbf{K}(L) = (K_{\mathrm{II}} \quad K_{\mathrm{I}} \quad K_{\mathrm{III}})^{\mathrm{T}} \tag{14}$$

and their relationship with the stresses $\mathbf{t}$ is

$$\mathbf{K}(L) = \sqrt{2\pi r} \cdot \mathbf{R}\left[\left(\frac{r}{L}\right)^{\mathrm{W}}\right] \cdot \mathbf{t}, \tag{15}$$

where [see Ting (1986)]

$$\gamma = \frac{1}{2\pi} \ln\left(\frac{1+\beta}{1-\beta}\right) \tag{16}$$

and

$$\beta = \{-\tfrac{1}{2}\,\mathrm{tr}[(\mathbf{WD}^{-1})^2]\}^{1/2}. \tag{17}$$

In eqn (17), $\mathbf{W}$ and $\mathbf{D}$ are the negative real and imaginary parts of a complex matrix $\mathbf{M}$, that is,

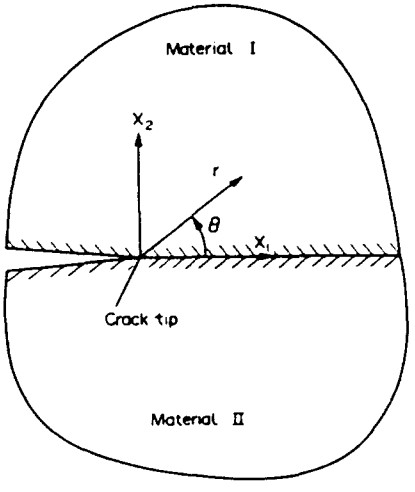

Fig. 1. An interface crack between dissimilar anisotropic media.

$$\mathbf{M} = -(\mathbf{W} + i\mathbf{D}) \tag{18}$$

and $\mathbf{M}$ in turn is related to a Hermitian matrix $\mathbf{A}$ which is defined by the elastic constants of the bimaterial. More specifically,

$$\mathbf{M} = -i(2\pi)^{1/2}[\mathbf{A}^{\mathrm{T}}]^{-1}, \tag{19}$$

$$\mathbf{A} = (\tilde{\mathbf{B}}^{\mathrm{I}} + \mathbf{B}^{\mathrm{II}})^{-1}, \tag{20}$$

$$\mathbf{B}^{\alpha} = i(2\pi)^{-1/2} \sum_{N=1}^{3} \mathrm{Adj}\, \mathbf{L}^{\alpha}(p_N^{\alpha}) \left[\sum_{M=1}^{3} \mathbf{C}^{\alpha}(p_M^{\alpha})\, \mathrm{Adj}\, \mathbf{L}^{\alpha}(p_M^{\alpha}) \right]^{-1}, \tag{21}$$

$$\mathbf{L}^{\alpha}(p_N^{\alpha}) = \mathbf{Q}^{\alpha} + p_N^{\alpha}[\mathbf{S}^{\alpha} + (\mathbf{S}^{\alpha})^{\mathrm{T}}] + p_N^{2}\mathbf{V}^{\alpha}, \tag{22}$$

$$\mathbf{C}^{\alpha}(p_N^{\alpha}) = (\mathbf{S}^{\alpha})^{\mathrm{T}} + p_N^{\alpha}\mathbf{V}^{\alpha}, \tag{23}$$

$$\alpha = \mathrm{I}, \mathrm{II},$$

where the superscript $\alpha = \mathrm{I}$ or II refers to material I or II, respectively.

It can be shown that (Ting, 1986)

$$-\tfrac{1}{2}\,\mathrm{tr}\,[(\mathbf{W}\mathbf{D}^{-1})^2] > 0 \tag{24}$$

so β in eqn (17) is always real. Also, in eqn (15), the matrix $\mathbf{R}$ is defined by

$$\mathbf{R}[c] = \mathbf{I} + \mathrm{Im}\,[c]\mathbf{P} + (1 - \mathrm{Re}\,[c])\mathbf{P}^2, \tag{25}$$

where Im and Re denote the imaginary and real parts, respectively, $\mathbf{I}$ is the unit matrix, and

$$\mathbf{P} = \frac{1}{\beta}\tilde{\mathbf{W}}\tilde{\mathbf{D}}^{-1}, \tag{26}$$

$$\mathbf{M}^{-1} = \tilde{\mathbf{W}} + i\tilde{\mathbf{D}}. \tag{27}$$

It should also be noted that $\mathbf{R}$ has the following properties:

$$\mathbf{R}[1] = \mathbf{I}, \tag{28a}$$

$$\mathbf{R}[c] \cdot \mathbf{R}[e] = \mathbf{R}[ce], \tag{28b}$$

in which the arguments c and e are dimensionless, so that $\mathbf{R}$ is also dimensionless.

For materials where the x_3-axis is a two-fold symmetry axis, the elastic constants $C_{\alpha\beta 23} = C_{\alpha\beta 31} = 0$ and $C_{2312} = C_{3112} = 0$. There is thus no coupling of the displacement component u_3 with the components u_1 and u_2. In this case, the matrix $\mathbf{P}^2$ in eqn (25) can be shown to be

$$\mathbf{P}^2 = -\begin{bmatrix} 1 & 0 & 0 \\ 0 & 1 & 0 \\ 0 & 0 & 0 \end{bmatrix}. \tag{29}$$

Also, σ_{23} and K_{III} disappear for plane problems, so only K_{I} and K_{II} need be considered. From eqns (29), (25) and (15), the stress intensity factors in terms of the stresses become

$$\mathbf{K}(L) = \begin{bmatrix} K_{II} \\ K_{I} \end{bmatrix} = \sqrt{2\pi r}\mathbf{R}'\left[\left(\frac{r}{L}\right)^{i\gamma}\right]\begin{bmatrix} \sigma_{12} \\ \sigma_{22} \end{bmatrix}. \tag{30}$$

where

$$\mathbf{R}'\left[\left(\frac{r}{L}\right)^{i\gamma}\right] = \mathrm{Re}\left[\left(\frac{r}{L}\right)^{i\gamma}\right]\mathbf{I} + \mathrm{Im}\left[\left(\frac{r}{L}\right)^{i\gamma}\right]\mathbf{P}$$

$$= \cos\left[\gamma \ln\left(\frac{r}{L}\right)\right]\begin{bmatrix} 1 & 0 \\ 0 & 1 \end{bmatrix} - \sin\left[\gamma \ln\left(\frac{r}{L}\right)\right]\begin{bmatrix} P_{11} & P_{12} \\ P_{21} & P_{22} \end{bmatrix}. \tag{31}$$

It is evident from eqns (30) and (31) that when $r \to 0$, the stresses exhibit an oscillatory singularity, as was mentioned earlier. In the case when $\gamma = 0$, that is, when the elastic body is homogeneous, $\mathbf{R}'$ becomes a unity matrix and the stress intensity factors are then of the classical separate form for the two distinct modes of crack deformation.

3. BEM DETERMINATION OF THE S.I.F.

The analytical basis of the BEM in elastostatics is the transformation of the governing partial differential equations valid over the entire elastic solution domain Ω into an integral equation written for just its boundary Γ. In the direct formulation, use of the unit load fundamental solutions with the Betti–Rayleigh reciprocal work theorem will, through appropriate limiting operations, result in the boundary integral equation (BIE) relating the displacements u_α and tractions t_α at Γ. The BIE for two dimensions may be written in indicial notation as:

$$C_{\alpha\beta}(P)u_\alpha(P) + \int_\Gamma u_\alpha(Q)T_{\alpha\beta}(P,Q)\,\mathrm{d}\Gamma(Q) = \int_\Gamma t_\alpha(Q)U_{\alpha\beta}(P,Q)\,\mathrm{d}\Gamma(Q), \quad \alpha,\beta = 1,2, \tag{32}$$

where $U_{\alpha\beta}(P,Q)$ and $T_{\alpha\beta}(P,Q)$ are the fundamental solutions which represent the displacements and tractions, respectively, in the x_β-direction at P in a plane homogeneous infinite body. Details of their derivation for the anisotropic case have been given by Cruse (1988) and their explicit forms have also been presented by Tan and Gao (1992). Also, in eqn (32), the value of $C_{\alpha\beta}(P)$ depends on the local geometry of Γ at the point P.

To solve the BIE numerically, the boundary Γ of the solution domain is divided into a series, or "mesh" of line elements. Over each of these elements, the boundary geometry, displacements and tractions may be written, as in the present work, in terms of their respective nodal values and the quadratic shape functions $N^c(\zeta)$. The elements each have three nodes, two at the ends and one at the mid-point; and the associated shape functions $N^c(\zeta)$ are

$$N^1(\zeta) = \tfrac{1}{2}\zeta(\zeta - 1),$$
$$N^2(\zeta) = 1 - \zeta^2,$$
$$N^3(\zeta) = \tfrac{1}{2}\zeta(1 + \zeta). \tag{33}$$

Substitution of the isoparametric representations of the geometry and functions into eqn (32) will result in a set of linear algebraic equations for the unknown tractions and displacements at the nodes on the boundary of the solution domain. These equations may then be solved using standard matrix solution techniques.

If the elastic domain is made up of several piece-wise different materials, it may be divided into several sub-regions, each with corresponding material properties. A BIE is written for each sub-region and the appropriate continuity and equilibrium conditions are applied at the common interface boundaries, before the linear algebraic equations are solved. This multi-region approach may also be used to model general crack problems in

homogeneous bodies (Blandford *et al.*, 1981) whereby a domain is divided into two or more sub-regions with the artificial interface boundaries containing the crack plane.

It has been well established in BEM linear elastic analysis of fracture problems that the use of the traction-singular quarter-point crack-tip elements will yield accurate results for the stress intensity factors [see, e.g. Martinez and Dominguez (1984), Tan and Gao (1990a, b, 1991, 1992)]. This is because the near-tip fields are more accurately represented over these elements. It has also been widely shown that by simply shifting the mid-point nodes of the quadratic isoparametric elements adjacent to the crack tip to the quarter-points (see Fig. 2), using the shape functions given in eqn (33), the following form of the variation for the displacements and tractions over the elements is obtained:

$$\left.\begin{matrix} u_\alpha \\ t_\alpha \end{matrix}\right\} = A_\alpha^{(1)} + A_\alpha^{(2)}\sqrt{\frac{r}{l}} + A_\alpha^{(3)}\left(\frac{r}{l}\right), \quad \alpha = 1, 2, \tag{34}$$

where the superscripts denote the nodes shown in Fig. 2, and l is the length of the crack-tip element. In addition, if the shape functions associated with the nodal tractions for the element ahead of the crack-tip, as shown in Fig. 2, are multiplied by $\sqrt{l/r}$, the tractions are $O(r^{-1/2})$. That is,

$$\begin{aligned} t_\alpha &= \left[A_\alpha^{(1)} + A_\alpha^{(2)}\sqrt{\frac{r}{l}} + A_\alpha^{(3)}\frac{r}{l}\right]\sqrt{\frac{l}{r}} \\ &= \bar{t}_\alpha^{(1)} N^1(\zeta)\sqrt{\frac{l}{r}} + \bar{t}_\alpha^{(2)} N^2(\zeta)\frac{l}{r} + \bar{t}_\alpha^{(3)} N^3(\zeta). \end{aligned} \tag{35}$$

It can be further verified that the computed nodal values of "tractions", $\bar{t}_\alpha^{(i)}$, on this traction singular element are related to the physical values $t_\alpha^{(i)}$ as follows:

$$\begin{aligned} \bar{t}_\alpha^{(1)} &= t_\alpha^{(1)}, \\ \bar{t}_\alpha^{(2)} &= \tfrac{1}{2} t_\alpha^{(2)}, \\ \bar{t}_\alpha^{(3)} &= \lim_{r \to 0} t_\alpha^{(3)}\sqrt{\frac{r}{l}}. \end{aligned} \tag{36}$$

For cracks in homogeneous materials, the bimaterial property $\gamma = 0$, eqn (31) then becomes

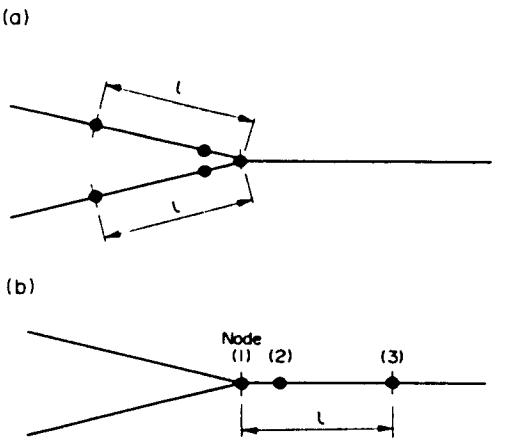

Fig. 2. Quarter-point crack tip elements: (a) on the crack faces; and (b) ahead of the crack tip.

$$\mathbf{R}'\left[\left(\frac{r}{l}\right)^{-i\varepsilon}\right] = \mathbf{I} = \begin{bmatrix} 1 & 0 \\ 0 & 1 \end{bmatrix}. \tag{37}$$

so

$$\mathbf{K}(L) = \mathbf{K} = \sqrt{2\pi r}\mathbf{t} = \sqrt{2\pi l}\tilde{\mathbf{t}}^{(1)}, \tag{38}$$

or

$$\begin{bmatrix} K_{\mathrm{II}} \\ K_{\mathrm{I}} \end{bmatrix} = \sqrt{2\pi l}\begin{bmatrix} \tilde{t}_1^{(1)} \\ \tilde{t}_2^{(1)} \end{bmatrix}. \tag{39}$$

in which the classical stress intensity factors are directly obtained from the computed nodal value of the traction coefficient $\tilde{t}_\alpha^{(1)}$ at the crack tip. In the case of interface cracks between dissimilar isotropic materials, $P_{11} = P_{22} = 0$ and $P_{12} = -P_{21} = 1$ in eqn (31). It then becomes

$$\mathbf{R}'\left[\left(\frac{r}{L}\right)^{-i\varepsilon}\right] = \cos\left[\gamma \ln\left(\frac{r}{L}\right)\right]\begin{bmatrix} 1 & 0 \\ 0 & 1 \end{bmatrix} - \sin\left[\gamma \ln\left(\frac{r}{L}\right)\right]\begin{bmatrix} 0 & 1 \\ -1 & 0 \end{bmatrix}, \tag{40}$$

which clearly has the oscillatory form as $r \to 0$. However, the modulus K_0 of the complex stress intensity factor, defined as

$$K_0 = |\mathbf{K}| = \sqrt{K_{\mathrm{I}}^2 + K_{\mathrm{II}}^2} \tag{41}$$

is not oscillatory in form. Besides, the strain energy release rate, G, which may generally be expressed as (Wu, 1990):

$$G = \tfrac{1}{4}\mathbf{K}^{\mathrm{T}}\tilde{\mathbf{D}}^{-1}\mathbf{K}, \tag{42}$$

can be shown to be directly proportional to K_0^2. This led the authors to determine K_0 instead of K_{I} and K_{II} directly in their previous studies (Tan and Gao, 1990a, b, 1991). From eqns (30), (36) and (40) K_0 can be shown to be related to the computed nodal traction coefficients as:

$$K_0 = \sqrt{2\pi l}\,[(\tilde{t}_1^{(1)})^2 + (\tilde{t}_2^{(1)})^2]^{1/2}. \tag{43}$$

For an interface crack between dissimilar anisotropic materials, $P_{\alpha\beta} \neq 0$, $(\alpha, \beta = 1, 2)$. It can then be easily verified using eqns (31) and (36) that K_0 will not have the same simple form of eqn (42) in terms of the computed traction coefficients. A new modified shape function is therefore introduced into eqn (35), which incorporates the oscillatory nature of the traction singularity at the interface crack-tip. The variation of the tractions over the singular quarter-point crack-tip element is now taken to be:

$$\begin{aligned} t_\alpha &= \mathbf{R}'\left[\left(\frac{r}{l}\right)^{i\varepsilon}\right]\cdot\left(\sqrt{\frac{l}{r}}\right)\cdot\left[A_\alpha^{(1)} + A_\alpha^{(2)}\left(\sqrt{\frac{r}{l}}\right) + A_\alpha^{(3)}\left(\frac{r}{l}\right)\right] \\ &= N^1(\zeta)\cdot\sqrt{\frac{l}{r}}\cdot\mathbf{R}'\left[\left(\frac{r}{l}\right)^{i\varepsilon}\right]\cdot\hat{t}_\alpha^{(1)} + N^2(\zeta)\cdot\left(\frac{l}{r}\right)\cdot\mathbf{R}'\left[\left(\frac{r}{l}\right)^{i\varepsilon}\right]\cdot\hat{t}_\alpha^{(2)} + N^3(\zeta)\cdot\mathbf{R}'\left[\left(\frac{r}{l}\right)^{i\varepsilon}\right]\cdot\hat{t}_\alpha^{(3)}, \end{aligned} \tag{44}$$

where $\hat{t}_\alpha^c$ is the computed traction coefficient at the cth node of the crack-tip element with this new modified shape function. It can be easily verified that the relationship between $\hat{t}_\alpha^c$ and the physical tractions t_α^c is as follows:

$$\hat{t}_x^{(3)} = t_x^{(3)},$$

$$\hat{t}_x^{(2)} = \tfrac{1}{2}\mathbf{R}'[(\tfrac{1}{2})^{-i\varepsilon}] \cdot t_x^{(2)},$$

$$\hat{t}_x^{(3)} = \lim_{r \to 0} \sqrt{\frac{r}{l}} \cdot \mathbf{R}'\left[\left(\frac{r}{l}\right)^{-i\varepsilon}\right] \cdot t_x^{(1)}. \tag{45}$$

For two different characteristic dimensions L_1 and L_2, the corresponding stress intensity factors $\mathbf{K}(L_1)$ and $\mathbf{K}(L_2)$ may be related according to Wu (1990):

$$\mathbf{K}(L_1) = \mathbf{R}'\left[\left(\frac{L_1}{L_2}\right)^{i\varepsilon}\right] \cdot \mathbf{K}(L_2). \tag{46}$$

Thus, from eqns (28), (30), (45) and (46), using the crack-tip element length l, as one of the characteristic dimensions,

$$\begin{aligned}\mathbf{K}(L) &= \mathbf{R}'\left[\left(\frac{L}{l}\right)^{i\varepsilon}\right]\mathbf{K}(l) \\ &= \mathbf{R}'\left[\left(\frac{L}{l}\right)^{i\varepsilon}\right] \cdot \sqrt{2\pi r} \cdot \mathbf{R}'\left[\left(\frac{r}{l}\right)^{-i\varepsilon}\right] \cdot \sqrt{\frac{l}{r}} \cdot \mathbf{R}\left[\left(\frac{r}{l}\right)^{i\varepsilon}\right] \cdot \hat{t}^{(1)} \\ &= \mathbf{R}'\left[\left(\frac{L}{l}\right)^{i\varepsilon}\right] \cdot \sqrt{2\pi l} \cdot \hat{\mathbf{t}}^{(1)},\end{aligned} \tag{47}$$

where $\hat{\mathbf{t}}^{(1)} = [\hat{t}_1^{(1)} \ \hat{t}_2^{(1)}]^{\mathrm{T}}$ are the computed traction coefficients at the crack-tip node. Equation (47) may be written explicitly as

$$\begin{bmatrix} K_{\mathrm{II}}(L) \\ K_{\mathrm{I}}(L) \end{bmatrix} = \sqrt{2\pi l} \cdot \mathbf{R}'\left[\left(\frac{L}{l}\right)^{i\varepsilon}\right] \cdot \begin{bmatrix} \hat{t}_1^{(1)} \\ \hat{t}_2^{(1)} \end{bmatrix}. \tag{48}$$

As can be seen from this equation, the numerical difficulties associated with the oscillatory singularity are now removed. Furthermore, it enables the stress intensity factors to be obtained directly and simply from the BEM computed traction coefficients at the crack-tip node.

4. NUMERICAL EXAMPLES

The results for four test problems, all with exact analytical solutions, are presented here to demonstrate the veracity of the BEM approach described above for obtaining stress intensity factors of bimaterial interface cracks. Of these four problems, isotropic bimaterials were treated in two of them. This was, in part, to verify the soundness of the technique when the material properties reduce to the case of isotropy, and also because of the paucity of exact closed-form solutions for anisotropic bimaterial interface cracks. In addition to these test problems, one other problem was treated in this study to illustrate a typical application of the method, such as in the micromechanics analysis of multi-phase materials. It involves an elliptical inclusion with a debond crack in an anisotropic matrix.

In the numerical treatment of the problems, all the quadratic quarter-point crack-tip elements have the same length l for a given problem case. This length l was typically taken to be 10% of the modelled crack length a. The elements adjacent to these crack-tip elements were gradually increased in size away from the crack-tip along the bimaterial interface. As will be seen below, a relatively small number of boundary elements was used for each of these problems considered. All the computations were carried out on the Honeywell DPS8/70 computer using single precision arithmetic.

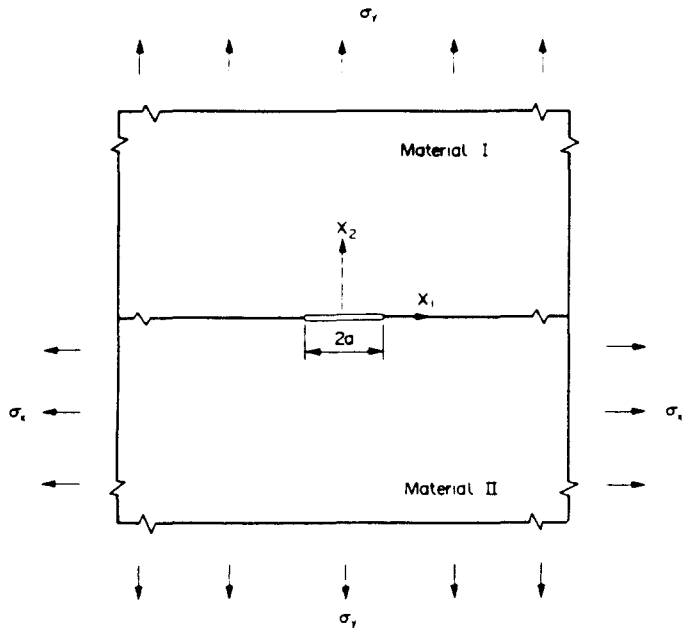

Fig. 3. Infinite isotropic bimaterial plate with an interface crack subjected to remote direct stresses — Problem (i).

Problem (i): An interface crack in an infinite isotropic bimaterial plate

Figure 3 shows the first test problem treated, namely, that of an infinite isotropic bimaterial plate with an interface crack of length $2a$, subjected to direct stresses at infinity. In the BEM model, a finite bimaterial plate was considered instead, but its height and width were taken to be 20 times the size of the crack. Thus the effects of the finite boundaries can be expected to be not significant. The problem was analysed under conditions of plane stress. Also, with reference to Fig. 3, the applied stress σ_x was taken to be $[\nu_2-(E_2/E_1)\nu_1](\sigma_y)$, where E_α and ν_α are the Young's modulus and Poisson's ratio, respectively, of material α. This was to ensure continuity conditions for the strain ε_{11} along the bimaterial interface. The boundary element mesh employed for this problem is shown in Fig. 4 where only half of

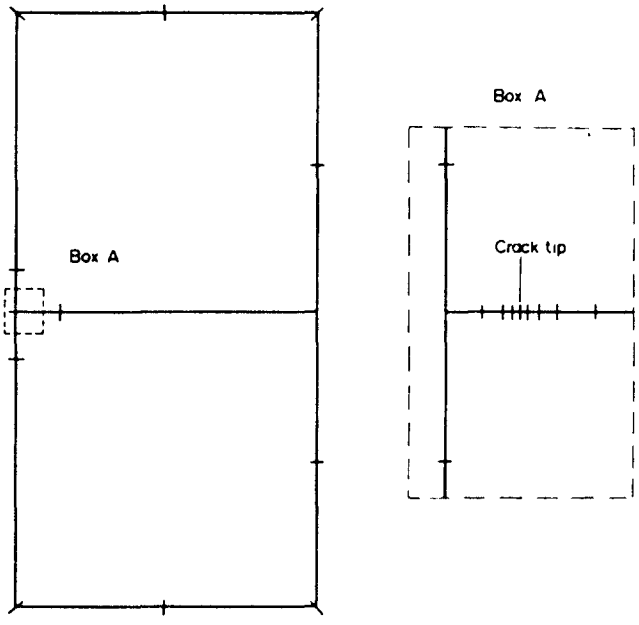

Fig. 4. BEM mesh for Problem (i).

Table 1. Normalized stress intensity factors for an interface crack on an infinite bimaterial isotropic plate under remote stresses—Problem (i)

E_1/E_2	γ	$K_I/\sigma_\infty\sqrt{\pi a}$			$K_{II}/\sigma_\infty\sqrt{\pi a}$		
		Exact	BEM	% Error	Exact	BEM	% Error
1	0	1.000	1.010	1.0	0	0	0
5	0.075	1.006	1.024	1.8	−0.098	−0.096	−2.0
20	0.104	1.013	1.031	1.8	−0.136	−0.141	3.7
100	0.114	1.015	1.017	0.2	−0.148	−0.155	4.7

the physical problem was modelled by virtue of symmetry. A total of 34 boundary elements and 68 nodes were used to represent the two sub-regions with the respective material properties. Four different values of E_1/E_2 were treated, namely, 1, 5, 20 and 100; the Poisson's ratios ν_1 and ν_2 were taken to be the same however, as 0.3. These ratios thus correspond to the following values for the bimaterial constant γ in eqn (16): 0, 0.075, 0.104 and 0.114, respectively.

The exact solution for this problem has been given by Rice and Sih (1965). Using eqn (48), the stress intensity factors K_I and K_{II} were obtained from the BEM computed traction coefficients at the crack-tip node of the traction-singular quarter-point element. The characteristic dimension L was taken to be equal to the half-crack length a in the calculations. Table 1 lists the normalized stress intensity factors, $K_I/\sigma_\infty\sqrt{\pi a}$ and $K_{II}/\sigma_\infty\sqrt{\pi a}$, as obtained from the BEM analysis for the different E_2/E_1 ratios considered. Also listed are the corresponding exact solutions of Rice and Sih (1965). As can be seen, the BEM results are very good indeed, with less than 2% error for K_I and less than 5% for K_{II}. The strain energy release rate, G, for the different cases was also calculated according to eqn (42) in the BEM study, and their non-dimensionalized values are shown plotted in Fig. 5 against the E_1/E_2 ratio with the closed form solution. The errors of the BEM results were again less than 5% for the range of the Young's moduli ratios treated.

Problem (ii): A debond crack between a circular inclusion and an infinite matrix

Figure 6 shows an isotropic, elastic circular inclusion, radius a, embedded in an infinite matrix which is made of another isotropic elastic material. A circular arc debond crack, spanning an angle 2θ exists as shown, between the two elastic media, and the matrix is subjected to remote biaxial tension σ. In the BEM analysis, the infinite body was modelled as a square with side lengths 20 times the diameter of the inclusion. Four different values of θ were treated, namely, $\theta = 30^\circ, 60^\circ, 90^\circ$ and 120°. For each of these angles, the same E_1/E_2 ratios as in the previous example, namely, 1, 5, 20 and 100, were again considered. The Poisson's ratios for both materials were also taken as 0.3 but plane strain conditions were assumed. The corresponding values of γ, the bimaterial constant, were thus 0, 0.061, 0.084 and 0.092, respectively. Figure 7 shows a typical BEM mesh used to model half of

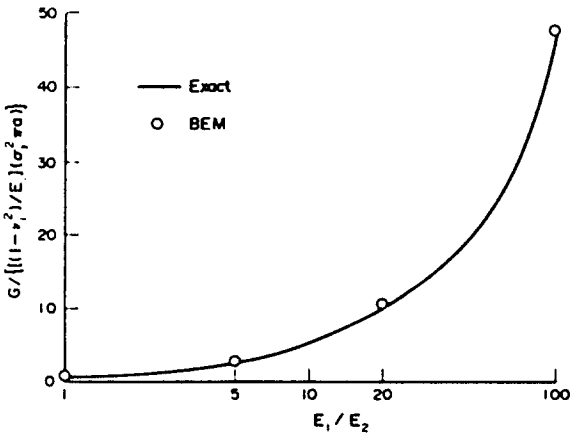

Fig. 5. Variation of the normalized strain energy release rate, $G/\{[(1-\nu_1^2)/E_1](\sigma_\infty\pi a)\}$ with the Young's modulus ratio, E_1/E_2—Problem (i).

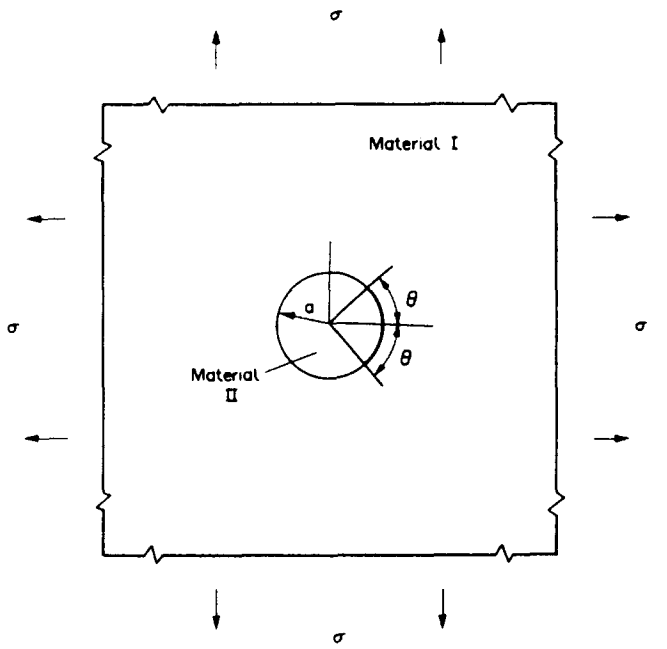

Fig. 6. An interface crack between a circular isotropic inclusion and an infinite isotropic matrix subject to biaxial tension—Problem (ii).

the physical problem, advantage being taken of symmetry. It has two sub-regions with a total of 35 boundary elements and 70 nodes.

Table 2 presents the BEM computed values of $K_I/\sigma\sqrt{\pi a}$ and $K_{II}/\sigma\sqrt{\pi a}$, and the corresponding exact results by Perlman and Sih (1967). The characteristic dimension L for the stress intensity factor computations was taken as a. As can be seen from the table, the magnitudes of the error in the BEM solutions were all within 5% for all the cases considered. This was also true for the computed strain energy release rate, G, the variations of which with E_1/E_2 for the different values of θ are shown in Fig. 8.

Problem (iii): An interface crack between dissimilar materials opened by internal pressure

The third test problem considered was that of a crack, length $2a$ and subjected to internal pressure σ_0 at its faces, which lie along the straight interface between two dissimilar

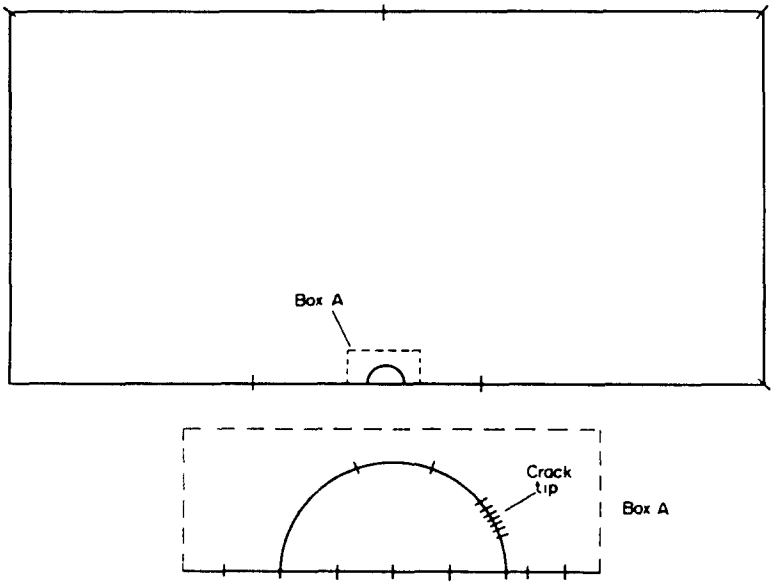

Fig. 7. BEM mesh for Problem (ii).

Table 2. Normalized stress intensity factors for a circular arc crack lying along the interface of an isotropic elastic inclusion in an infinite isotropic body—Problem (ii)

			$K_I/\sigma_\infty\sqrt{\pi a}$			$K_{II}/\sigma_\infty\sqrt{\pi a}$		
θ	E_1/E_2	γ	Exact	BEM	% Error	Exact	BEM	% Error
30	1	0	0.640	0.625	−2.3	−0.172	−0.166	−3.5
	5	0.061	0.884	0.859	−2.8	−0.124	−0.126	1.4
	20	0.084	0.938	0.934	−0.4	−0.089	−0.091	2.2
	100	0.092	0.953	0.955	0.2	−0.077	−0.077	0
60	1	0	0.644	0.631	−2.0	−0.372	−0.364	−2.2
	5	0.061	0.986	0.951	−3.5	−0.459	−0.448	−2.4
	20	0.084	1.080	1.069	−1.0	−0.460	−0.456	−0.9
	100	0.092	1.106	1.105	−0.1	−0.457	−0.452	−1.1
90	1	0	0.471	0.463	−1.7	−0.471	−0.457	−3.0
	5	0.061	0.797	0.779	−2.3	−0.680	−0.664	−2.4
	20	0.084	0.918	0.912	−0.7	−0.738	−0.725	−1.2
	100	0.092	0.957	0.957	0	−0.754	−0.739	−2.0
120	1	0	0.265	0.261	−1.5	−0.460	−0.442	−3.9
	5	0.061	0.497	0.497	0	−0.708	−0.707	−0.1
	20	0.084	0.610	0.613	0.5	−0.813	−0.802	−1.4
	100	0.092	0.653	0.657	0.6	−0.851	−0.829	−2.6

semi-infinite bodies, as shown in Fig. 9. In this problem, material 1 was treated as anisotropic with the orthogonal material axes, x_1^*-x_2^*, rotated by an angle θ with respect to the global x_1-x_2 axes, as shown in the figure. To reduce the number of variable parameters in the problem, material 2 was treated as isotropic. It should, however, be emphasized that this does not detract from the validity of the BEM technique employed. For the purpose of illustration, the elastic properties of single crystal alumina Al_2O_3 were used for material 1, while those of fully stabilized polycrystal zirconia, FSP ZrO_2, were used for material 2. The engineering constants for the former, calculated from the elastic compliances given in Simmons and Wang (1971), are as follows:

$$E_{11}^* = 345\ \text{GPa}, \quad E_{22}^* = 516\ \text{GPa}, \quad E_{33}^* = 345\ \text{GPa},$$
$$\nu_{12}^* = 0.131, \quad \nu_{13}^* = 0.362, \quad \nu_{23}^* = 0.196,$$
$$\eta_{12,1}^* = 59\ \text{GPa}, \quad \eta_{12,2}^* = 0, \quad \eta_{12,3}^* = -59\ \text{GPa},$$
$$G_{12}^* = 173\ \text{GPa},$$

where the asterisks denote that these values are with reference to the orthogonal material axes directions; E_{kk}^* is the Young's modulus in the x_k^*-direction; G_{12}^* is the shear modulus

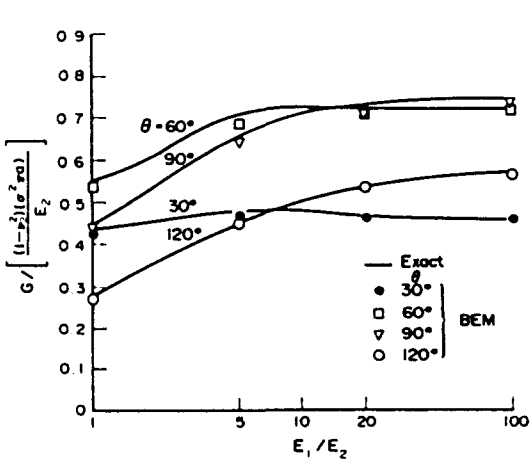

Fig. 8. Variation of the normalized strain energy release rate, $G/\{[(1-\nu_1^2)/E_1](\sigma^2\pi a)\}$ with the Young's modulus ratio E_1/E_2—Problem (ii).

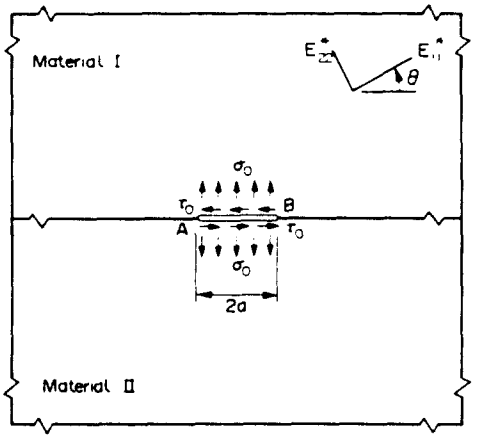

Fig. 9. An interface crack between anisotropic alumina and FSP zirconia—Problems (iii) and (iv).

in the x_1^*–x_2^* plane; ν_{jk}^* is the Poisson's ratio which is defined as the compressive strain in the x_k^*-direction due to a unit extensional strain in the x_j^*-direction; and the quantities $\eta_{jk,k}^*$ are referred to by Lekhnitskii (1963) as the coefficients of mutual influence of the first kind. As a matter of interest, the isotropic values for the Young's modulus and Poisson's ratio of Al_2O_3 have been given in the literature as 396 GPa and 0.24, respectively. As for the FSP zirconia, which is isotropic, the corresponding values are 192 GPa and 0.3, respectively.

In the numerical analysis, a finite bimaterial body was treated with width W and height $2H$ equal to $20a$. Figure 10 shows the boundary element mesh employed for the problem; it has a total of 46 elements and 92 nodes. Plane strain conditions were again assumed in the analysis. Also, four different values of θ, the angle of orientation of the material axes, were considered, namely, $\theta = 0°$, 30°, 60° and 90°. The exact closed-form solution for the

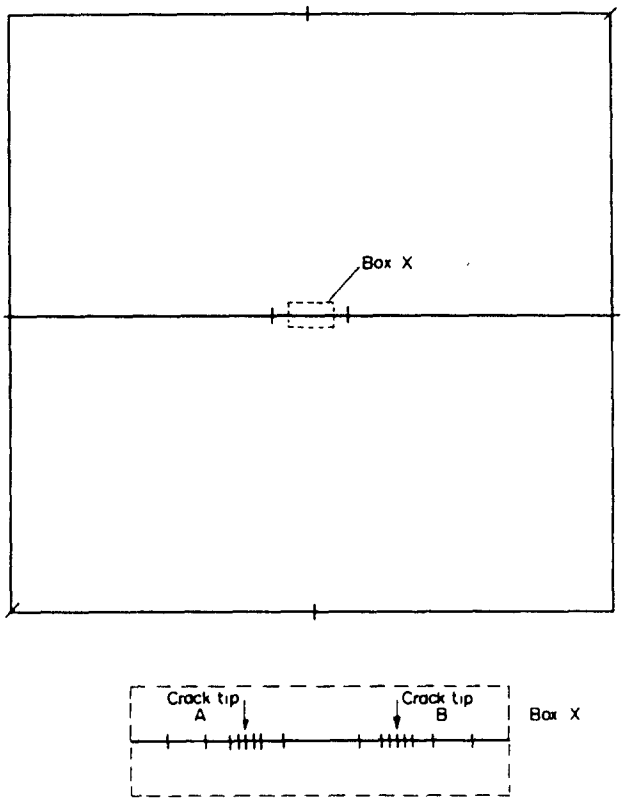

Fig. 10. BEM mesh for problems (iii) and (iv).

Table 3. Normalized stress intensity factors and strain energy release rates for a pressurized interface crack between FSP ZrO_2 and anisotropic Al_2O_3 half-planes. $\bar{K} = \sigma_0\sqrt{\pi a}$; $G_0 = \frac{1}{4}(\bar{d}_{11}+\bar{d}_{12}+\bar{d}_{21}+\bar{d}_{22})|_{\theta=0}\bar{K}^2$

θ	γ		Exact	BEM	% Error
0	0.0254	$K_I^A/\bar{K}$	0.992	1.000	0.8
		$K_I^B/\bar{K}$	0.999	0.992	−0.7
		$K_{II}^A/\bar{K}$	0.107	0.101	5.6
		$K_{II}^B/\bar{K}$	−0.107	−0.107	0.0
		G^A/G_0	0.478	0.485	1.4
		G^B/G_0	0.479	0.483	0.8
30	0.0443	$K_I^A/\bar{K}$	0.979	0.994	1.5
		$K_I^B/\bar{K}$	0.992	1.005	1.3
		$K_{II}^A/\bar{K}$	0.193	0.186	−3.6
		$K_{II}^B/\bar{K}$	−0.193	−0.186	−3.6
		G^A/G_0	0.478	0.491	2.7
		G^B/G_0	0.479	0.489	2.1
60	0.0078	$K_I^A/\bar{K}$	1.000	1.005	0.5
		$K_I^B/\bar{K}$	1.000	1.003	0.3
		$K_{II}^A/\bar{K}$	0.035	0.033	−5.7
		$K_{II}^B/\bar{K}$	−0.035	−0.033	−5.7
		G^A/G_0	0.522	0.526	0.8
		G^B/G_0	0.522	0.525	0.6
90	0.0254	$K_I^A/\bar{K}$	0.999	1.006	0.7
		$K_I^B/\bar{K}$	0.992	0.998	0.6
		$K_{II}^A/\bar{K}$	0.111	0.105	−5.4
		$K_{II}^B/\bar{K}$	−0.111	−0.105	−5.4
		G^A/G_0	0.496	0.502	1.2
		G^B/G_0	0.495	0.500	1.0

stress intensity factors of interface cracks between anisotropic dissimilar half planes has been given by Wu (1990). Thus, the accuracy of the BEM solutions can be assessed with respect to these results. This is shown in Table 3, where the superscripts "A" and "B" in K_I, K_{II} and G denote the two crack tips shown in Fig. 9. The characterizing dimension L used in the stress intensity factor computations here was W, the width of the bimaterial plate. Also, the parameter G_0 used for non-dimensioning the strain energy release rate G is

$$G_0 = \tfrac{1}{4}(\bar{d}_{11}+\bar{d}_{12}+\bar{d}_{21}+\bar{d}_{22})|_{\theta=0}(\sigma_0^2\pi a), \tag{49}$$

where $\bar{d}_{\alpha\beta}$ are the coefficients of the $\bar{D}$ matrix defined in eqn (27) and are material parameters. For the single crystal properties of Al_2O_3 considered, when $\theta = 0^\circ$, they are as follows:

$$\begin{aligned} \bar{d}_{11} &= 1.375\times10^{-2}, \quad & \bar{d}_{12} &= 4.041\times10^{-4}, \\ \bar{d}_{21} &= 4.041\times10^{-4}, \quad & \bar{d}_{22} &= 1.328\times10^{-2}. \end{aligned} \tag{50}$$

The accuracy of the BEM results for K_I and G can be seen to be very good indeed, the errors were all less than 3%. Those for K_{II} were slightly higher however, but then, the numerical values of K_{II} are about an order of magnitude smaller than K_I for this problem. It is also evident from the results that, for a given BEM mesh employed, the accuracy of the solutions obtained was not dependent on the orientation of the material axes, as should be the case.

Problem (iv): An interface crack subjected to pure shear lying between dissimilar materials

The fourth test problem analysed was similar to that in Problem (iii) in all respects except for the loading condition on the crack faces. Instead of internal pressure acting on the crack faces, they were subjected to a uniform shear stress τ_0 as shown in Fig. 9. The boundary element mesh used was also the same as in the previous example,

Table 4. Normalized stress intensity factors and strain energy release rates for an interface crack subjected to shear stress, lying between FSP ZrO_2 and anisotropic Al_2O_3 half-planes. $\bar{K} = \tau_0\sqrt{\pi a}$; $G_0 = \frac{1}{4}(d_{11}+d_{12}+d_{21}+d_{22})|_{\theta=0}\bar{K}^2$

θ	γ		Exact	BEM	% Error
0	0.0254	$K_I^A/\bar{K}$	−0.111	−0.104	−6.3
		$K_I^B/\bar{K}$	0.111	0.104	−6.3
		$K_{II}^A/\bar{K}$	0.999	1.006	0.7
		$K_{II}^B/\bar{K}$	0.992	0.998	0.6
		G^A/G_0	0.496	0.502	1.2
		G^B/G_0	0.495	0.500	1.0
30	0.0443	$K_I^A/\bar{K}$	−0.187	−0.179	−4.3
		$K_I^B/\bar{K}$	0.187	0.179	−4.3
		$K_{II}^A/\bar{K}$	0.992	1.006	1.4
		$K_{II}^B/\bar{K}$	0.979	0.992	1.3
		G^A/G_0	0.464	0.475	2.4
		G^B/G_0	0.463	0.474	2.4
60	0.0078	$K_I^A/\bar{K}$	−0.032	−0.030	−6.3
		$K_I^B/\bar{K}$	0.032	0.030	−6.3
		$K_{II}^A/\bar{K}$	1.000	1.004	0.4
		$K_{II}^B/\bar{K}$	1.000	1.002	0.2
		G^A/G_0	0.485	0.489	0.8
		G^B/G_0	0.485	0.487	0.4
90	0.0254	$K_I^A/\bar{K}$	−0.107	−0.101	−5.6
		$K_I^B/\bar{K}$	0.107	0.103	−3.7
		$K_{II}^A/\bar{K}$	0.992	1.004	1.2
		$K_{II}^B/\bar{K}$	0.999	1.008	0.9
		G^A/G_0	0.478	0.484	1.2
		G^B/G_0	0.479	0.483	0.8

as shown in Fig. 10. Table 4 lists the results for the normalized stress intensity factors, $K_I/\tau_0\sqrt{\pi a}$ and $K_{II}/\tau_0\sqrt{\pi a}$, and the normalized strain energy release rate G/G_0, where $G_0 = (d_{11}+d_{12}+d_{21}+d_{22})(\tau_0^2\pi a)/4$. The coefficients $d_{\alpha\beta}$ have the same numerical values previously used. In this problem, the magnitudes of K_{II} are about an order greater than those of K_I. It is again of significance to note that the BEM results were very good indeed, thus validating the technique employed.

Problem (v): An elliptical inclusion with an interface crack in an anisotropic matrix

The final problem treated was that of an elliptical elastic inclusion embedded in an infinite anisotropic matrix and containing an interface debond crack as shown in Fig. 11. The geometry of the inclusion is defined by the semi-major and semi-minor axes, a and b, respectively, and the extent of the debond crack is measured by the angle 2θ. Also, the anisotropic matrix is subject to remote uniform radial tension σ. The elastic inclusion was taken to be FSP ZrO_2 here while the matrix was taken to have the same elastic properties of single crystal Al_2O_3 given earlier. Five different ellipse aspect ratios, b/a, were analysed, namely, $b/a = 1/3$, $1/2$, 1, 2 and 3. For each of these geometries, three sizes of the interface crack were treated; they correspond to $\theta = 30°$, 60° and 90°.

In the BEM analysis, the infinite matrix was modelled as a finite circular cylinder with radius $10a$. Also, the material axes directions were taken to coincide with those of the global Cartesian axes. For the purpose of comparison, repeat computer runs were made with the matrix assumed to be isotropic Al_2O_3 for each of the above-mentioned geometric cases. Figure 12 shows a typical BEM mesh employed for the problem where a maximum of 52 elements and 104 nodes were used.

The results for the stress intensity factors are shown in Table 5; they have been normalized with respect to $\sigma\sqrt{\pi a}$ and the characterizing dimension L used in their computations was a. It is worth noting from this table that the stress intensity factor K_I and K_{II} at the two crack-tips "A" and "B" can be significantly different from one another in magnitude because of the material anisotropy. They are also in deviation from the corresponding results obtained when the matrix was assumed to be isotropic. Figures 13(a),

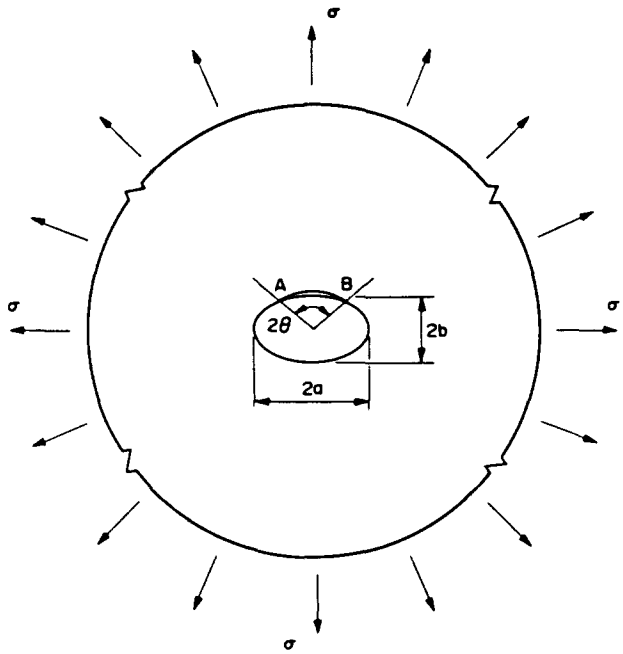

Fig. 11. An elliptical FSP ZrO_2 inclusion in an anisotropic Al_2O_3 matrix with an interface crack—Problem (v).

(b) and (c) show the variations of the normalized strain energy release rate with the aspect ratio, b/a, of the elliptical inclusion, for the three debond crack sizes analysed. The coefficients $\bar{d}_{\alpha\beta}$ in the normalizing parameter were the same as before as given in eqn (50). Of interest to note is that the strain energy release rate obtained for the isotropic matrix case was closer to that at crack-tip "B" in the anisotropic matrix case, for a given crack size.

5. CONCLUSIONS

The multi-region boundary element method (BEM) for plane anisotropy has been employed in the analysis of interface cracks between dissimilar materials. It was based

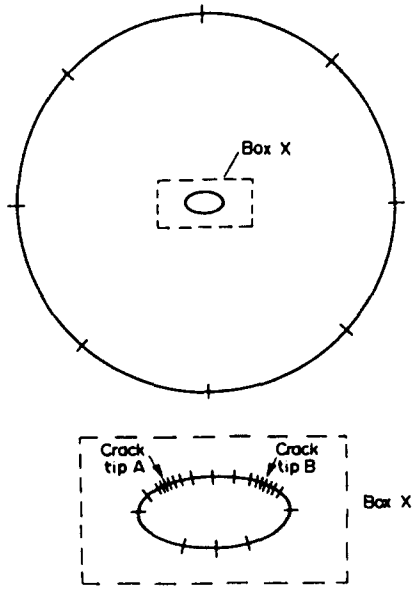

Fig. 12. BEM mesh for Problem (v).

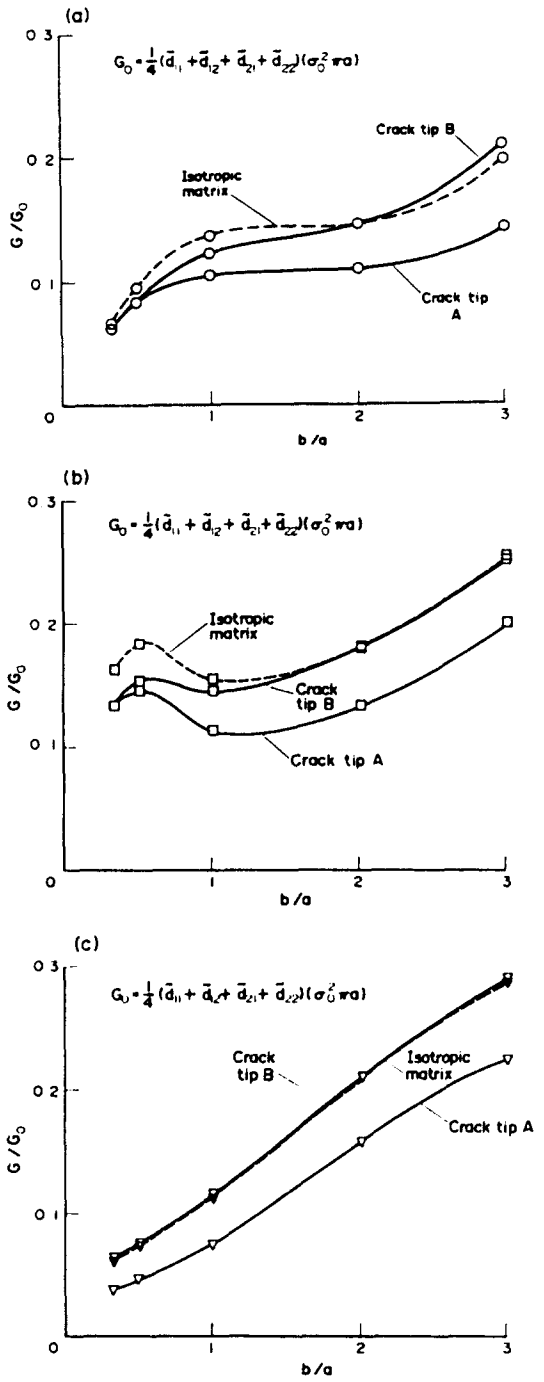

Fig. 13. Variation of the normalized strain energy release rate, G/G_0, with the ellipse aspect ratio, b/a, (a) for $\theta = 30^\circ$, (b) for $\theta = 60^\circ$, and (c) for $\theta = 90^\circ$.

on the quadratic isoparametric element formulation and special quarter-point crack-tip elements which incorporate the proper oscillatory $O(r^{-1/2+i\varepsilon})$ traction singularity were used. With these elements, a simple expression relating the stress intensity factors to the BEM computed nodal traction coefficients at the interface crack tip could be obtained. This provided a very quick and efficient means of obtaining the stress intensity factors for interface cracks between dissimilar anisotropic bodies. The technique was validated by four test problems in this paper, two of which have a crack between dissimilar isotropic materials while in the other two, material anisotropy was considered. Very good solution accuracy for the stress intensity factors and the energy release rates were obtained even with modest mesh discretizations. The results for a fifth problem, namely that of an elliptic elastic

Table 5. Normalized stress intensity factors for an interface crack between an elliptical FSP ZrO_2 zirconia inclusion and an infinite alumina Al_2O_3 matrix subjected to uniform radial tension—Problem (v). $\bar{K} = \sigma\sqrt{\pi a}$
(NOTE: For the isotropic matrix, K_{II} is +ve for crack-tip A; −ve for crack-tip B.)

		Anisotropic matrix				Isotropic matrix	
θ	b/a	$K_I^A/\bar{K}$	$K_{II}^A/\bar{K}$	$K_I^B/\bar{K}$	$K_{II}^B/\bar{K}$	K_I	K_{II} (±)
30	1/3	0.325	0.142	0.358	−0.047	0.369	0.039
	1/2	0.412	0.022	0.411	−0.092	0.429	0.059
	1	0.408	0.260	0.482	−0.116	0.494	0.155
	2	0.405	0.239	0.443	−0.266	0.462	0.279
	3	0.429	0.396	0.594	−0.241	0.536	0.314
60	1/3	0.526	0.009	0.520	−0.145	0.556	0.094
	1/2	0.543	0.059	0.530	−0.239	0.580	0.159
	1	0.420	0.225	0.503	−0.236	0.469	0.291
	2	0.439	0.286	0.531	−0.332	0.495	0.334
	3	0.583	0.263	0.620	−0.412	0.610	0.363
90	1/3	0.135	0.229	0.273	−0.249	0.200	0.281
	1/2	0.174	0.248	0.283	−0.283	0.221	0.305
	1	0.273	0.280	0.369	−0.330	0.320	0.338
	2	0.442	0.352	0.547	−0.388	0.498	0.406
	3	0.584	0.341	0.689	−0.381	0.641	0.392

inclusion in an anisotropic matrix and containing an interface debond crack, have also been presented. It provided an illustration of the practical usefulness of the boundary element method in the fracture mechanics analysis of multi-phase materials even in anisotropy.

REFERENCES

Bassani, J. L. and Qu, J. (1989a). Finite crack on bimaterial and bicrystal interfaces. *J. Mech. Phys. Solids* **37**, 435–453.

Bassani, J. L. and Qu, J. (1989b). On elasticity solutions for cracks on bimaterial and bicrystal interfaces. *Mater. Sci. Engng* **A107**, 177–184.

Blandford, G. E., Ingraffea, A. R. and Liggett, J. A. (1981). Two dimensional stress intensity factor computations using the boundary element method. *Int. J. Numer. Meth. Engng* **17**, 387–404.

Cao, H. C. and Evans, A. G. (1989). An experimental study of the fracture resistance of bimaterial interfaces. *Mech. Mater.* **7**, 295–304.

Charalambides, P. G., Lund, J., Evans, A. G. and McMeeking, R. M. (1989). A test specimen for determining the fracture resistance of bimaterial interfaces. *J. Appl. Mech.* **56**, 77–82.

Clements, D. L. (1971). A crack between dissimilar anisotropic media. *Int. J. Engng Sci.* **9**, 257–265.

Comninou, M. (1977). The interface crack. *J. Appl. Mech.* **44**, 631–636.

Comninou, M. (1990). An overview of interface cracks. *Engng Fract. Mech.* **37**, 197–208.

Cruse, T. A. (1988). *Boundary Element Analysis in Computational Fracture Mechanics*. Kluwer Academic Publishers, Dordrecht, The Netherlands.

England, A. H. (1965). A crack between dissimilar media. *J. Appl. Mech.* **32**, 400–402.

Erdogan, F. (1965). Stress distribution in bonded dissimilar materials with cracks. *J. Appl. Mech.* **32**, 403–410.

Gao, Y. L. and Tan, C. L. (1992). Determination of characterizing parameters for bimaterial interface cracks using the boundary element method. *Engng Fract. Mech.* **41**, 779–784.

Hasebe, N., Okumura, M. and Nakamura, T. (1987). Stress analysis of debonding and a crack around a circular rigid inclusion. *Int. J. Fract.* **32**, 169–183.

Hutchinson, J. W. and Evans, A. G. (1989). On the mixed mode fracture resistance of interfaces. *Acta Mettall.* **37**, 909–916.

Kaeznski, A. and Matysiak, S. J. (1989). A system of interface cracks in periodically layered elastic composite. *Engng Fract. Mech.* **32**, 745–756.

Kuo, A. Y. and Wang, S. S. (1985). A dynamic finite element analysis of interfacial cracks in composites. In *Delamination and Debonding of Materials*, ASTM STP 876, pp. 5–34.

Lee, K. Y. and Choi, H. J. (1988). Boundary element analysis of stress intensity factors for bimaterial interface cracks. *Engng Fract. Mech.* **29**, 461–472.

Lekhnitskii, S. G. (1963). *Theory of Elasticity of an Anisotropic Elastic Body*. Holden-Day, San Francisco.

Lin, K. Y. and Hartmann (1989). Numerical analysis of stress singularities at a bonded anisotropic wedge. *Engng Fract. Mech.* **32**, 211–224.

Martinez, J. and Dominguez, J. (1984). On the use of quarter-point boundary elements for stress intensity factor computations. *Int. J. Numer. Meth. Engng* **20**, 1941–1950.

Matos, P. P. L., McMeeking, R. M., Charalambides, P. G. and Drory, M. D. (1989). A method for calculating stress intensities in bimaterial fracture. *Int. J. Fract.* **40**, 235–254.

Nakagawa, K., Anma, T. and Duan, S. J. (1990). A mathematical approach of the interface crack between dissimilar anisotropic composite materials. *Engng Fract. Mech.* **36**, 439–449.

Ni, L. and Nemat-Nasser, S. (1991). Interface cracks in anisotropic dissimilar materials: an analytic solution. *J. Mech. Phys. Solids* **39**, 113–114.
Park, J. H. and Earmme, Y. Y. (1986). Application of conservation integrals to interfacial crack problems. *Mech. Mater.* **5**, 261–276.
Perlman, A. B. and Sih, G. C. (1967). Elastostatic problems of curvilinear cracks in bonded dissimilar materials. *Int. J. Engng Sci.* **5**, 845–867.
Raju, I. S., Crews, J. H. and Aminpour, M. A. (1988). Convergence of strain energy release rate components for edge-delaminated composite laminates. *Engng Fract. Mech.* **30**, 383–396.
Rice, J. R. (1988). Elastic fracture mechanics concepts for interfacial cracks. *J. Appl. Mech.* **55**, 98–103.
Rice, J. R. and Sih, G. C. (1965). Plane problems of cracks in dissimilar media. *J. Appl. Mech.* **32**, 418–423.
Simmons, G. and Wang, H. (1971). *Single Crystal Elastic Constants and Calculated Aggregate Properties, A Handbook*. MIT Press, Cambridge, MA.
Sun, C. T. and Jih C. J. (1987). On strain energy release rates for interfacial cracks in bimaterial media. *Engng Fract. Mech.* **28**, 13–20.
Sun, C. T. and Manoharan, M. G. (1989). Strain energy release rates of an interfacial crack between two orthotropic solids. *J. Comp. Mater.* **23**, 460–478.
Tan, C. L. and Gao, Y. L. (1990a). Treatment of bimaterial interface crack problems using the boundary element method. *Engng Fract. Mech.* **36**, 919–932.
Tan, C. L. and Gao, Y. L. (1990b). Stress intensity factors for cracks at spherical inclusions by the boundary integral equation method. *J. Strain Anal.* **25**, 197–206.
Tan, C. L. and Gao, Y. L. (1991). Axisymmetric boundary integral equation analysis of interface cracks between dissimilar materials. *Computational Mech.* **7**, 381–396.
Tan, C. L. and Gao, Y. L. (1992). Boundary element analysis of plane anisotropic bodies with stress concentrations and cracks. *Int. J. Comp. Struct.* **20**, 17–28.
Ting, T. C. T. (1986). Explicit solution and invariance of the singularities at an interface crack in anisotropic composites. *Int. J. Solids Structures* **22**, 965–983.
Toya, M. (1990). Fracture mechanics of interfaces. *Int. J. JSME* **33 Series I**, 413–424.
Wang, S. S. and Yuan, F. G. (1983). A hybrid finite element approach to composite laminate elasticity problems with singularities. *J. Appl. Mech.* **50**, 835–844.
Williams, M. L. (1959). The stresses around a fault or crack in dissimilar media. *Bull. Seismol. Soc. Am.* **49**, 199–204.
Willis, J. R. (1971). Fracture mechanics of interfacial cracks. *J. Mech. Phys. Solids* **19**, 353–368.
Wu, K. C. (1990). Stress intensity factor and energy release rate for interfacial cracks between dissimilar anisotropic materials. *J. Appl. Mech.* **57**, 882–886.
Wu, K. C. (1991). Explicit crack-tip fields of an extending interface crack in an anisotropic bimaterial. *Int. J. Solids Structures* **27**, 455–466.
Yehia, N. A. B. and Sheppard, M. S. (1988). Automatic crack growth tracking of bimaterial interface cracks. *Int. J. Fract.* **37**, 123–135.
Yuuki, R. and Cho, S. B. (1989). Efficient boundary element analysis of stress intensity factors for interface cracks in dissimilar materials. *Engng Fract. Mech.* **30**, 179–188.
Yuuki, R., Cho, S. B., Matsumoto, T. and Kisu, H. (1987). Usefulness of Hetenyi's solution for boundary element analysis of crack problems in dissimilar materials. In *Role of Fracture Mechanics in Modern Technology* (Edited by G. C. Sih, H. Nisitani and T. Ishihara), pp. 823–834. Elsevier, Amsterdam.